Proceedings of the 2021 Conference on Smart Materials, Adaptive Structures and Intelligent Systems
SMASIS2021
September 14-15, 2021, Virtual, Online

SMASIS2021-68384

WORK CAPACITY OF SELF-FOLDING POLYMER ORIGAMI

Ryan Long
Auburn University
Auburn, Alabama

Deepika Singla
Auburn University
Auburn, Alabama

Kanak Parmar
Auburn University
Auburn, Alabama

Manuel Indaco
Auburn University
Auburn, Alabama

Will Taylor
Auburn University
Auburn, Alabama

Nathan Adkins
Auburn University
Auburn, Alabama

Davide Guzzetti
Auburn University
Auburn, Alabama

Russell W. Mailen
Auburn University
Auburn, Alabama

ABSTRACT

Self-folding origami utilizes shape memory polymers (SMPs) to enable deployable space structures, such as those intended for large-scale, low-frequency radio interferometry. The size of structure that may be deployed is limited by the capacity of the smart material to do work. Previous studies focused on activation mechanisms and the kinematics of self-folding polymers, but have largely neglected an evaluation of the energy stored in the folding hinge. This paper seeks to characterize the work done by self-folding origami hinges made of pre-strained polystyrene (PSPS) as it deforms due to the shape-memory effect. SMP samples are patterned with black ink hinges and exposed to an infrared (IR) light. The ink absorbs thermal energy from the light, which leads to local heating and shrinking in the hinge region. Activation of the self-folding response, e.g. shrinking, occurs when the material reaches a temperature higher than its glass transition temperature, and a gradient in shrinking causes the sample to fold. The self-folding process is sensitive to physical constraints and changes in energy input into the sample. Thus, we will evaluate the energy stored in the self-folding hinge by measuring the work done under varying thermal stimuli in an array of tests that include universal material shrinkage and single-hinge folds. We evaluate hinge torque based on a dynamic analysis of the motion of the self-folding sheet. Quantification of the capacity of self-folding origami hinges to do work enables the design of deployable space structures by not only considering the activation mechanism and self-folding kinematics, but also accounts for the size of structure that may be deployed.

Keywords: Origami, Shape Memory Polymer, Self-folding

NOMENCLATURE

I	mass moment of inertia
PSPS	pre-strained polystyrene
SMP	shape memory polymer
T_g	glass transition temperature
α	coefficient of thermal expansion
θ	angular position
$\dot{\theta} = \frac{d\theta}{dt}$	angular velocity
$\ddot{\theta} = \frac{d^2\theta}{dt^2}$	angular acceleration

1. INTRODUCTION

Shape memory polymers (SMPs) enable thermally activated deployment mechanisms for large-scale, but light-weight, space structures. Thermomechanically induced pre-strain in SMPs enables the material to shrink as a result of viscoelastic strain recovery when the material is heated above the glass transition temperature, T_g. This process, known as self-folding origami, enables novel deployment methods that convert initially flat sheets into three-dimensional objects. In self-folding origami, the shape memory effect is concentrated into small discrete regions referred to as hinges. Self-folding hinges are pre-programmed into the material in a pattern that determines the final three-dimensional shape. Approaches to self-folding origami include patterned sheets **[1,2]** and layered composites **[3]** and may utilize activation stimuli such as IR light **[4]**, uniform heating Joule heating **[5]**, or lasers **[6]**. Not all of these approaches are suited to deployment of large structures such as the James Webb Space Telescope or the recently deployed Roll Out Solar Array (ROSA). In the case of spacecraft component design, availability of fold-initiating stimuli, material density,

and predictability of fold behavior are significant. This means mechanisms requiring highly controlled environments to activate, such as approaches involving uniform heating or exposure to aqueous solutions are not viable in **[7–10]**. Design of gossamer structures also requires consideration of the forces required to rotate large section of spacecraft during deployment or regular operation. Even a thin membrane structure such as a solar sail may require a relatively large force to orient due to its size.

A critical consideration in the self-folding of large deployable structures is the ability of the hinge to exert sufficient torque to fold the structure. Previous attempts to evaluate self-folding hinge torque include lifting of a mass **[5]** and quantifying the stress field variation across the thickness of the fold **[11]**. However, these investigations have not evaluated the capacity to do work of homogeneous, self-folding polymer sheets patterned with ink hinges.

Our approach to self-folding origami utilizes pre-strained polystyrene sheets (PSPS) that shrink to approximately 50% of their original size in both planar dimensions when heated above T_g (103°C **[4]**). These sheets can be patterned with black ink hinges using a conventional inkjet printer or marker. The PSPS is transparent to IR light, but the ink absorbs thermal energy from the IR light and converts it to heat. The heat conducts through the thickness, which creates a gradient in temperature. Wherever the material exceeds T_g, the material begins to shrink. Due to the gradient in temperature, there is a gradient in shrinkage, and the sample folds along the hinge. The folding behavior is influenced by initial heating of the sample, hinge width, and IR light intensity **[12–15]**. In the present study, we will conduct a series of experiments to evaluate the self-folding performance and hinge torque of such structures. We will use a dynamic mechanical analyzer (DMA) to evaluate the axial force generated in uniformly heated samples using isothermal and linear heating rate experiments. After evaluating the axial contracting force, we will evaluate the ability of SMP samples to self-fold in two configurations: (1) working against gravity and (2) oriented to minimize the effects of gravity but with increased moment of inertia. In the latter set of experiments, we will utilize lead weights to modify the mass moment of inertia of the sample, which will enable a more thorough characterization of the hinge torque.

This paper is organized as follows. In the Methods section, we will describe our material system, approach to patterning samples, and apparatus for self-folding. We will also develop an analytical model that allows us to convert angular position to hinge torque. In the Results section, we will present results for three experimental conditions. The first set of results are for uniaxial contraction tests subjected to isothermal and linear temperature ramp conditions. The second and third results will be for self-folding of samples oriented such that they are either folding against gravity or folding while minimizing gravity effects. The paper ends with a Discussion of the experimental results and Conclusions deduced from the data.

2. MATERIALS AND METHODS

2.1 Axial Contraction Tests

SMP samples are cut to dimensions of approximately 12.5 x 25 x 0.26 mm and tested in a TA Instruments HR-20 Hybrid Rheometer/DMA with environmental test chamber (ETC). The thin film tension fixture is used to evaluate axial contraction forces in the sample, and the gage length of the sample between the grips was set to 15 mm. The ETC enables control of sample temperature and heating rate above ambient conditions. In the experiments, samples were loaded into the test fixture, and a conditioning step is used to set the axial force to zero. The temperature in the ETC is then ramped to 90°C, at which point the sample is thermally soaked for 180 seconds. After thermal soaking, data recording and the temperature in the ETC is increased at a rate of 5°C/min to the target temperature of 120°C, 130°C, or 140 °C, which are representative of experimentally measured self-folding temperatures. The experiments output axial stress as a function of time.

2.2 Self-folding Tests

Samples are trimmed rectangles of Grafix Shrink Film, a commercially available film of PSPS approximately 0.27 mm thick. Patterning of sample hinges was done using a desktop inkjet printer. This ink is sufficiently dark for absorption of IR to initiate self-folding in PSPS. A standard Sharpie Permanent Marker, which does not encourage a self-folding behavior, was used for non-hinge patterning, such as labels and darkening required for video processing.

During testing, samples were clamped into a rotating fixture, allowing them to lie flat for pre-heating before being positioned during tests. Samples are positioned to face the array of 250 W IR bulbs while their edge is pointed towards the camera viewing the test. This allows the camera to capture the motion of the sample during the test with minimal distortion. The video is then processed using an edge detection approach to convert video of the test into angular position vs time data. By taking the derivative of this data twice, the angular acceleration can be found. Example images from this process are shown in **Figure 1**.

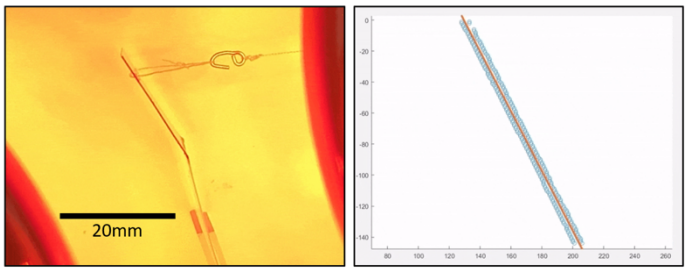

Figure 1 Raw video showing a top-down view of the full sample mid-test (left). The detected edge points in blue displayed as a scatter plot with a red line of best fit, the slope of this line will be used to calculate the angular position of the sample in this frame (right).

The angular acceleration is used to estimate the torque in the hinge according to

$$T = \ddot{\theta}(I + mL^2) \quad (1)$$

Where $\ddot{\theta}$ is the angular acceleration, I is the mass moment of inertia of the folding face and the final mL^2 term represents additional mass inertia added to the sample for certain tests (cf. **Figure 2**). For the sake of dimensional clarification, the sample dimensions to be referenced are shown in **Figure 3**.

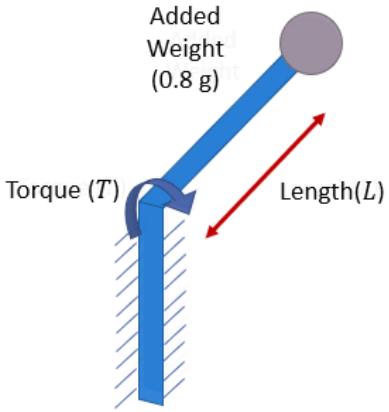

Figure 2: Force balance diagram of the weight-added load case, with the motion of sample, colored blue, folding occurring in the horizontal plane with the added resistance of weights attached to the moving face

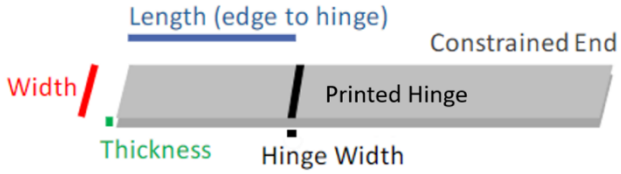

Figure 3: A simple ink hinge which will self-fold towards the printed line when exposed to IR.

3. RESULTS AND DISCUSSION

3.1 Uniaxial Contraction

Results from the uniaxial contraction force tests are shown in **Figure 4**. In this plot, the vertical dashed line represents the time at which T_g is achieved. A horizontal dashed line at a stress of zero is provided for reference. It is seen that, during initial heating, there is an axial stress that peaks between 1.5 and 2 MPa. This stress peak is associated with thermal expansion and subsequent buckling of the constrained sample. Note that the positive stress has to do with the sample pressing upward against the transducer. As the samples continue to heat through T_g, they begin to contract, and the buckled mode shape disappears. Between 200 and 400 seconds, the stress becomes negative, indicating that the sample is now pulling downward against the pressure transducer. The solid datapoints in the plot indicate the time at which the maximum temperature for each experiment is achieved. It is observed that the maximum negative stress occurs between 400 and 600 seconds. Beyond this local minimum, the stress in the samples decays towards zero. The rate of decay is higher for higher temperatures, as expected for a viscoelastic material. This region of negative stress represents the portion of the material shape recovery capable of performing work. At the end of each experiment, the sample has contracted visibly as shown in **Figure 5**. The samples are unloaded from the test fixture at the end of each experiment.

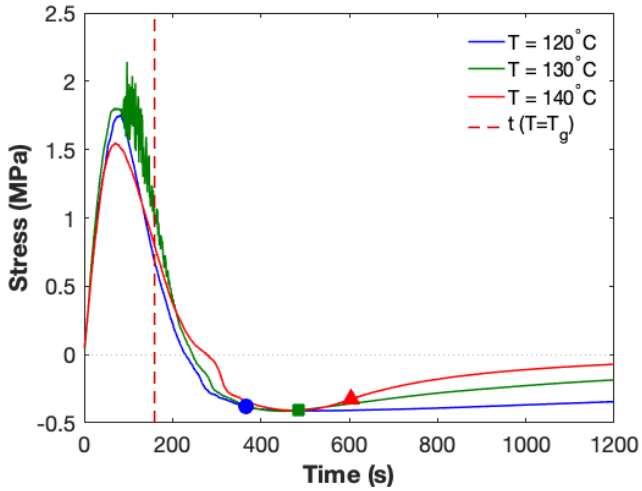

Figure 4: *Stress results for uniaxial contraction. Positive stress indicates compression of sample. The vertical dashed line represents the time at which T_g is exceeded. The discrete points represent the time at which the maximum temperature is achieved.*

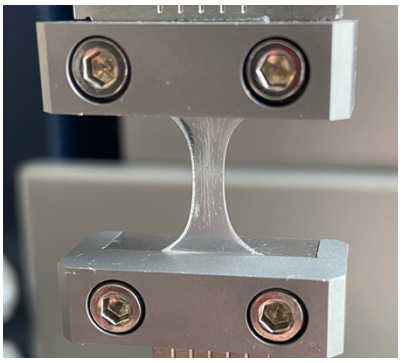

Figure 5 *Closeup of sample in thin film tension fixture. Note the lateral contraction of the sample between the grips.*

In support of the discussion above, the critical buckling stress of the sample has been calculated. The thermal stress can be estimated according to

$$\sigma_{th} = E\alpha\Delta T \quad (2)$$

Where the modulus of elasticity E = 1.78e9 Pa, α= 2.09e-4 K^-1, and ΔT ranges from 30°C - 50°C (use 130°C for calculations). The estimated thermal stress is thus 14.9 MPa. The critical buckling stress can be estimated according to

$$\sigma_{cr} = \frac{\pi^2 E}{K\left(\frac{L}{r}\right)^2} \quad (3)$$

Where r = $\sqrt{I/A}$ is the radius of gyration, K is an effective length factor (use 0.5 for fixed-fixed condition) and L = 15 mm is the

gage length of the sample. The estimated buckling stress is thus 1.76 MPa, which agrees well with the results shown in **Figure 4**.

3.2 Folding Against Gravity

The first set of folding tests conducted involve the sample lifting the free moving face against the force of gravity. **Figure 6** shows the effect of hinge width on the fold behavior, with higher acceleration and torque apparent when the surface area of the hinge is increased. The damping caused by the polymeric material moving past itself is responsible for the rapid deceleration that follows the initial acceleration.

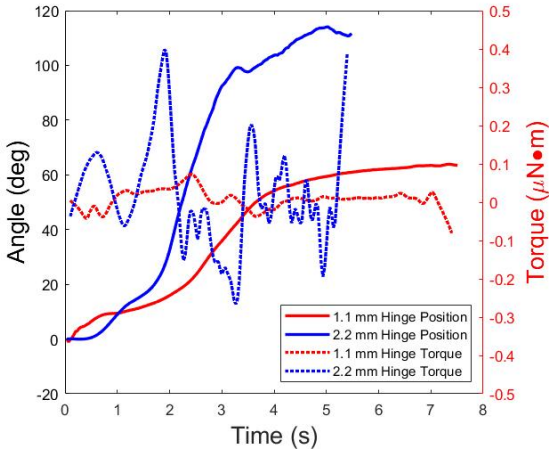

Figure 6: *A comparison of position and torque data over time for two lifting cases against gravity with identical dimensions except for hinge width.*

Another method for increasing the area of the hinge is to increase the width of the entire sample. As shown in **Figure 7**, this also creates an increase in peak torque. It also results in faster folding, which can also be attributed to the higher flux of energy into the sample made possible by the larger patterned area.

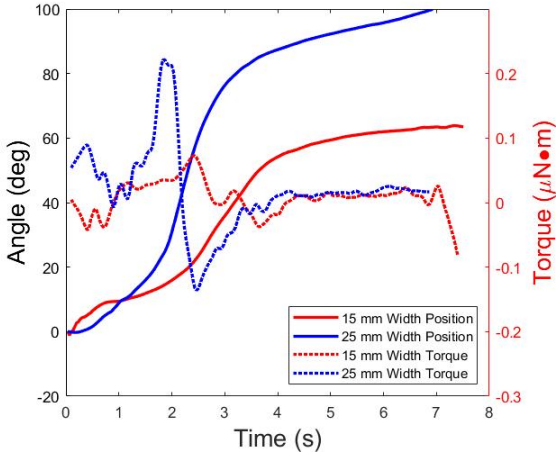

Figure 7: *A comparison of position and torque data over time for two lifting cases against gravity with identical dimensions except for sample width.*

3.3 Folding Without Gravity

Next, we attempt to reduce the effects of gravity by rotating the sample 90° so that it is not folding against gravity. In **Figure 8** and **Figure 9**, we evaluate the effects of hinge width and sample width respectively. Similar trends are observed as for the previous case, wherein increasing the surface area of the hinge results in faster folding and higher torque.

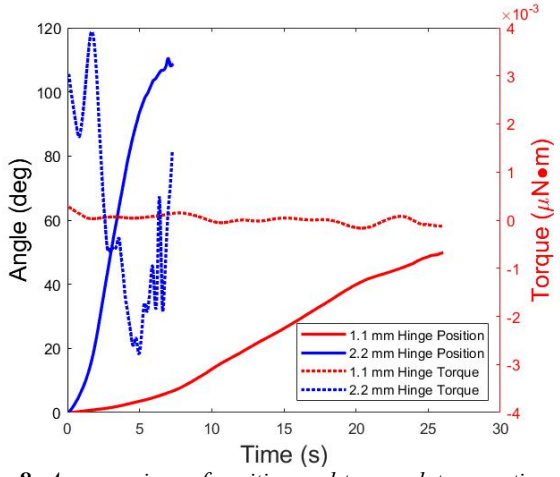

Figure 8: *A comparison of position and torque data over time for two lifting cases with samples rotated to mitigate the effect of gravity. Samples have identical dimensions except for hinge width.*

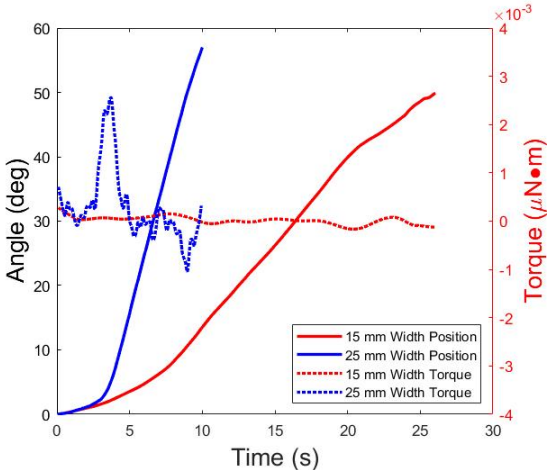

Figure 9: *A comparison of position and torque data over time for two lifting cases rotated to mitigate the effect of gravity on samples with identical dimensions except for sample width.*

In our final set of experiments, we attempt to modify the torque required to fold the sample by adding weight to the sample as illustrated in Figure 3. Again, we compare the effects of hinge width and sample width in **Figure 10** and **Figure 11**, respectively. Of note in **Figure 10** is the relatively low peak torque in the 1.1 mm hinge sample compared to the 2.2 mm sample. The smoother, almost linearly increasing position data explains how there is relatively little variation in acceleration, of which torque is a function.

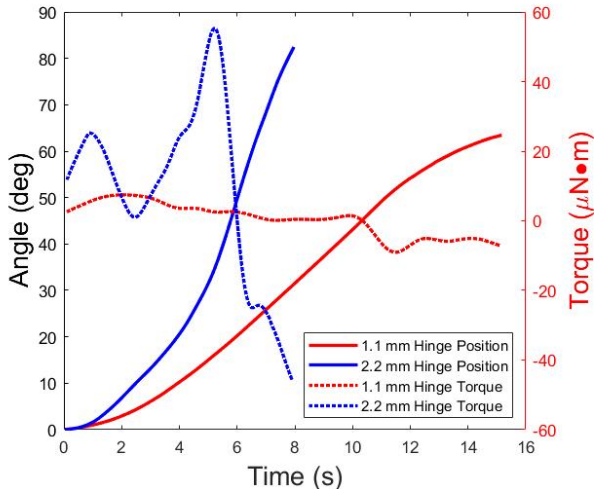

Figure 10: *A comparison of position and torque data over time for two samples rotated to mitigate the effect of gravity on samples with identical dimensions except for hinge width.*

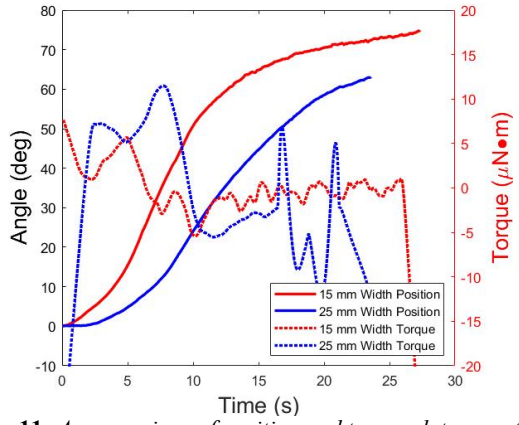

Figure 11: *A comparison of position and torque data over time for two weight-lifting cases rotated to mitigate the effect of gravity on samples with identical dimensions except for sample width.*

In **Figure 11**, the 25 mm wide sample exhibits a higher peak torque, similar to the results presented earlier. However, in this test, the 25 mm wide sample did not fold faster than the 15 mm wide sample. This is the only occurrence of this behavior observed and appears to be an example of how the sample behaves differently when moving much more weight than the sample weight.

In the preceding cases, the average mass of the moving face was 0.16 g, while the attached weights averaged 0.8 g. **Figure 12** is comprised of five weight moving tests using similar weight but with increasing distance from the hinge to the weight. The hinge width for all samples is 1.1 mm. The increase in moment arm results in a higher mass moment of inertia, I. In **Table 1**, the peak torque values, moment arm lengths, and calculated mass moment of inertia values are presented. An apparent behavior in these cases is that increases in the moment of inertia of the weighted moving face corresponds to longer duration fold times to reach the same angle, as demonstrated in ***Figure 12***. These slower folds at higher moments of inertia correspond to higher peak torque values. In other words, although the 30 mm moment arm folds slower than 10 mm moment arm in **Figure 12**, the torque is higher due to the increased moment of inertia.

Table 1: Summary of Hinge Torque Values

Peak Torque ($mN \cdot m$)	Moment Arm (mm)	I (kg m^2)
2.26	10	0.0667
4.24	15	0.156
7.45	20	0.358
12.61	25	0.574
11.73	30	0.718

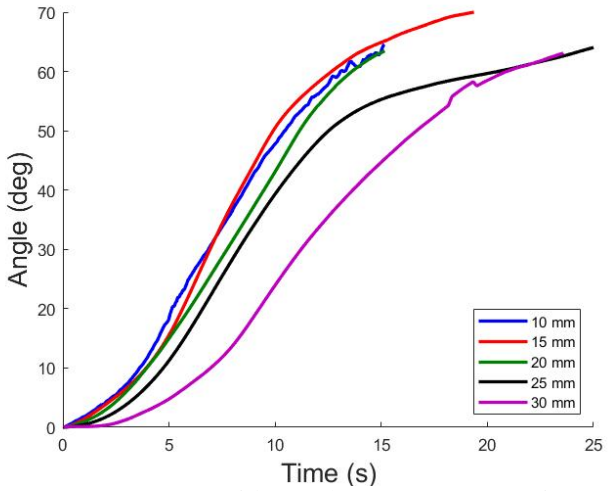

Figure 12: *A comparison of the angular position over time for a 1.1 mm wide hinge and five face lengths moving a 0.8 g weight.*

4. CONCLUSION

In this paper, we investigated the hinge torque in self-folding origami samples. Samples are patterned with black ink and exposed to IR light to induce folding. A relationship between the angular position as a function of time and the hinge torque was developed. In general, it was observed that increasing the surface area of the hinge, e.g. increased hinge width or sample width, resulted in faster folding and higher torque. Additionally, it was observed that samples which folded against gravity or some additional mass had greatly increased torque, which is attributed to damping by the polymer in unloaded samples. Future work will focus on controlling the precision of these behaviors, by controlling factors such as the sample's prestrain amount.

ACKNOWLEDGEMENTS

This work was completed at Auburn University under NASA grant 80NSSC20K1017.

REFERENCES

[1] Liu, Y., Genzer, J., and Dickey, M. D., 2016, "'2D or Not 2D': Shape-Programming Polymer Sheets," Progress in Polymer Science, **52**, pp. 79–106.

[2] Cui, X., Chen, J., Zhu, Y., and Jiang, W., 2020, "Natural Sunlight-Actuated Shape Memory Materials with Reversible Shape Change and Self-Healing Abilities Based on Carbon Nanotubes Filled Conductive Polymer Composites," Chem. Eng. J., **382**, p. 122823.

[3] Felton, S., Tolley, M., Demaine, E., Rus, D., and Wood, R., 2014, "A Method for Building Self-Folding Machines," Science, **345**(6197), pp. 644–646.

[4] Mailen, R. W., Liu, Y., Dickey, M. D., Zikry, M., and Genzer, J., 2015, "Modelling of Shape Memory Polymer Sheets That Self-Fold in Response to Localized Heating," Soft Matter, **11**(39), pp. 7827–7834.

[5] Felton, S. M., Tolley, M. T., Shin, B., Onal, C. D., Demaine, E. D., Rus, D., and Wood, R. J., 2013, "Self-Folding with Shape Memory Composites," Soft Matter, **9**(32), pp. 7688–7694.

[6] "Microfabricating 3D Structures by Laser Origami" [Online]. Available: https://www.spie.org/news/3952-microfabricating-3d-structures-by-laser-origami. [Accessed: 22-Apr-2021].

[7] Tolley, M. T., Felton, S. M., Miyashita, S., Aukes, D., Rus, D., and Wood, R. J., 2014, "Self-Folding Origami: Shape Memory Composites Activated by Uniform Heating," Smart Mater. Struct., **23**(9), p. 094006.

[8] Chen, T., Bilal, O. R., Lang, R., Daraio, C., and Shea, K., 2019, "Autonomous Deployment of a Solar Panel Using Elastic Origami and Distributed Shape-Memory-Polymer Actuators," Phys. Rev. Applied, **11**(6), p. 064069.

[9] Wu, R., Roberts, P. C. E., Lyu, S., Soutis, C., Zheng, F., Diver, C., Gresil, M., and Blaker, J. J., 2018, "Rigidisation of Deployable Space Polymer Membranes by Heat-Activated Self-Folding," Smart Mater. Struct., **27**(10), p. 105037.

[10] Danielson, C., Mehrnezhad, A., Yekrang Safakar, A., and Park, K., 2017, "Fabrication and Characterization of Self-Folding Thermoplastic Sheets Using Unbalanced Thermal Shrinkage," Soft Matter, **13**(23), pp. 4224–4230.

[11] Neville, R. M., Chen, J., Guo, X., Zhang, F., Wang, W., Dobah, Y., Scarpa, F., Leng, J., and Peng, H.-X., 2017, "A Kirigami Shape Memory Polymer Honeycomb Concept for Deployment," Smart Mater. Struct., **26**(5), p. 05LT03.

[12] Liu, Y., Boyles, J. K., Genzer, J., and Dickey, M. D., 2012, "Self-Folding of Polymer Sheets Using Local Light Absorption," Soft Matter, **8**(6), pp. 1764–1769.

[13] Liu, Y., Mailen, R., Zhu, Y., Dickey, M. D., and Genzer, J., 2014, "Simple Geometric Model to Describe Self-Folding of Polymer Sheets," Phys. Rev. E, **89**(4), p. 042601.

[14] Zhang, Q., Wommer, J., O'Rourke, C., Teitelman, J., Tang, Y., Robison, J., Lin, G., and Yin, J., 2017, "Origami and Kirigami Inspired Self-Folding for Programming Three-Dimensional Shape Shifting of Polymer Sheets with Light," Extreme Mechanics Letters, **11**, pp. 111–120.

[15] Lee, Y., Lee, H., Hwang, T., Lee, J., and Cho, M., 2015, "Sequential Folding Using Light-Activated Polystyrene Sheet," Scientific Reports, **5**, p. 16544.